



Wave-driven circulation in a coastal bay during the landfall of a hurricane

Ryan P. Mulligan,¹ Alex E. Hay,¹ and Anthony J. Bowen¹

Received 10 August 2007; revised 12 January 2008; accepted 7 February 2008; published 22 May 2008.

[1] A coupled wave/flow model was used to simulate the currents in a coastal bay during the landfall of a hurricane with large waves. Extensive wave breaking along the shoreline and over a midbay shoal induced the development of a strong mean circulation in the bay, in combination with currents forced by wind, tide, and storm surge. The general circulation pattern consisted of inflows along the shoreline and over the shoal region that were driven by radiation stress gradients, and outflows due to mass balance of the wave-driven inflow that were observed in deeper channels. The predicted currents agreed with observations only when wave forcing was included in the circulation model. Wave-driven flows accounted for over 50% of the high flushing rates during the storm and induced strong horizontal velocity gradients over short (~ 200 m) length scales.

Citation: Mulligan, R. P., A. E. Hay, and A. J. Bowen (2008), Wave-driven circulation in a coastal bay during the landfall of a hurricane, *J. Geophys. Res.*, 113, C05026, doi:10.1029/2007JC004500.

1. Introduction

[2] Many studies of waves, currents and their interactions have been conducted in nearshore regions, especially in relation to longshore currents and rip currents. *Longuet-Higgins and Stewart* [1964] described the forcing of currents and water level changes by gradients in wave momentum flux, or ‘radiation stress’. It has been shown that storm wave events play an important role in circulation along beaches [*Bowen*, 1969; *Feddersen and Guza*, 2003] and over coral reefs [*Symonds et al.*, 1995; *Kraines et al.*, 1998; *Gourlay and Colleter*, 2005]. The present study examines the forcing of currents by radiation stress gradients in a small $O(10$ km) semienclosed coastal bay.

[3] The study site is Lunenburg Bay, on the southern shore of Nova Scotia (Figure 1), approximately 8 km long and 4 km wide with a typical depth of 10 m. The bathymetry is irregular and the bay is exposed to waves from the North Atlantic Ocean from easterly and southerly directions. *Sturley and Bowen* [1996] developed a circulation model for Lunenburg Bay, capable of simulating the flow exchanges between the bay and attached coves. The three-dimensional nonlinear barotropic model was tidally forced and important advective processes in the system were identified including an ebb-tidal jet. *Sheng and Wang* [2003, 2004] developed a three-dimensional nonlinear circulation model of Lunenburg Bay forced by tides, wind and remotely generated long shelf waves. Their studies investigated nonlinear interactions between the forcing terms and influence on the development of currents. Tidal currents near the mouth of the bay were shown to be weak, $O(0.1$ m/s).

Wang et al. [2007] used this model to investigate the effects of wind, tidal and shelf-wave forcing during Hurricane Juan, the same event for which simulations are presented here. Their model was unable to account for the strong observed currents at all locations. None of the above models included surface gravity waves in the forcing of mean currents.

[4] In the present study, we examine the hypothesis that surface gravity wave forcing played a major role in the bay circulation during Hurricane Juan. Wave forcing is included in a circulation model in addition to forcing by winds, tides and the storm surge that occurred during the landfall of the hurricane. Observations are presented in section 2, and the numerical models are described in section 3. Model results and the importance of wave-driven flows on the bay circulation and flushing rates are explained in section 4, and conclusions are presented in section 5.

2. Observations

[5] Hurricane Juan formed as a tropical depression on 25 September 2003 at approximately 30° N latitude. It accelerated northward toward Nova Scotia, making landfall on 29 September 2003 at approximately 0300 UTC accompanied by strong winds and large waves. In Lunenburg Bay, the winds, water levels, waves and currents were observed by several instruments, part of the real-time coastal observing system set up under the Centre for Marine Environmental Prediction (www.cmep.ca) at Dalhousie University. The instrument stations, listed in Table 1 and shown in Figure 1, included an offshore directional waverider buoy (site *D*), two Acoustic Doppler Current Profilers (ADCPs) capable of measuring wave spectra (sites *A* and 1), two Acoustic Doppler Profilers (ADPs) with collocated pressure sensors (sites 2 and 3) and three electromagnetic S4 bottom current meters (sites 4–6). The wave buoy and pressure sensors sampled continuously, and all acoustic instruments sampled for 20 min every half hour except at site *A*, which

¹Department of Oceanography, Dalhousie University, Halifax, Nova Scotia, Canada.

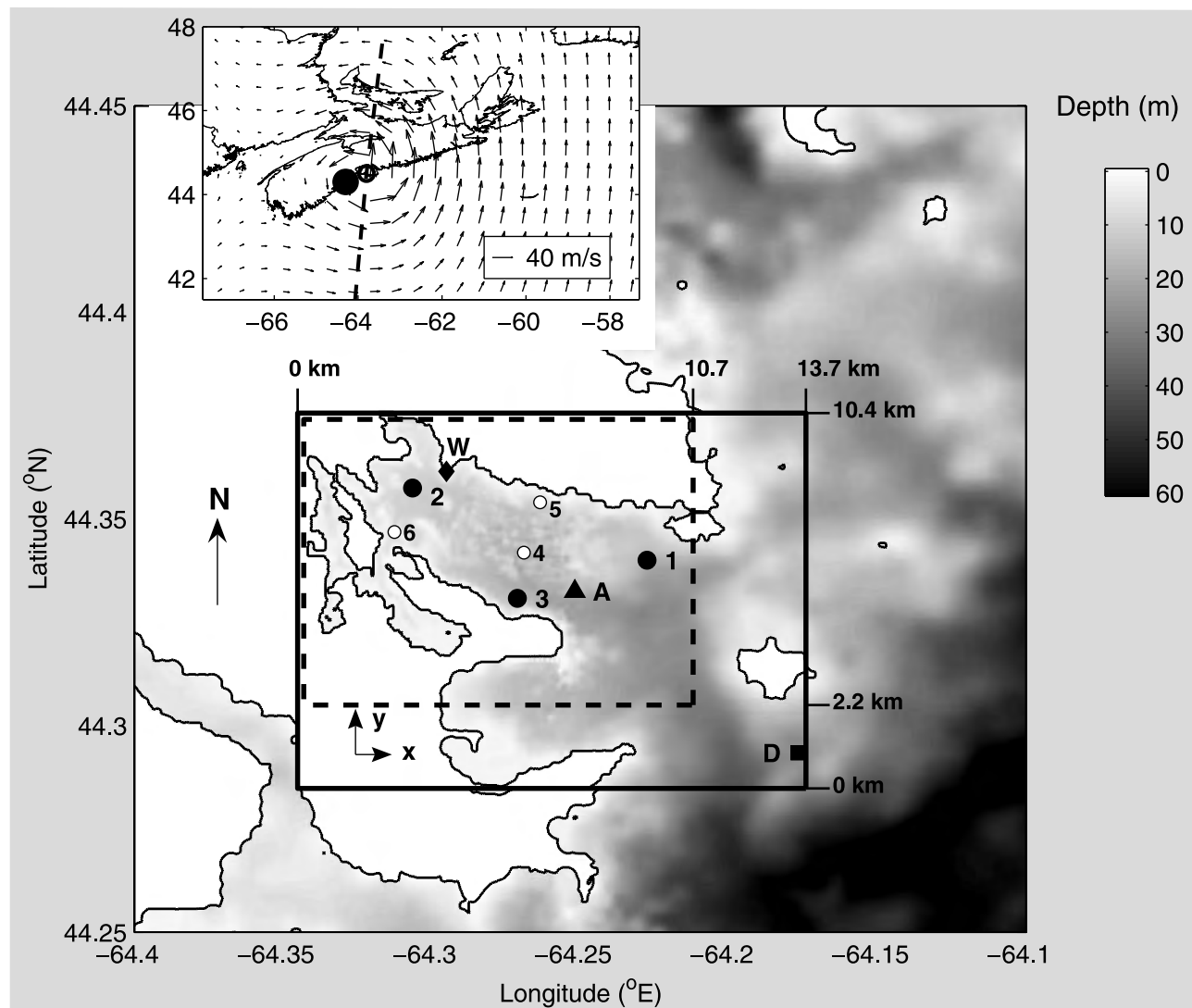


Figure 1. Lunenburg Bay bathymetry and instrument locations in 2003: D, DataWell directional waverider buoy; A, RDI Waves ADCP; numbers 1–3, surface meteorological buoys with bottom pods (RDI Waves ADCP at 1; Sontek ADP and Seabird PT sensor at 2 and 3); numbers 4–6, bottom pods with S4 current meters; and W, a meteorological shore station. The wave model domain is shown by the solid box; the smaller flow model domain is shown by the dashed box. Depths are relative to the low-water tidal datum, 1.3 m below mean sea level. Inset shows the location of Lunenburg Bay (black dot), the track of Hurricane Juan across Nova Scotia (dashed line), and wind vectors (60-km spacing) at landfall determined from the vortex wind model.

sampled for 30 min every two hours. The electromagnetic instruments sampled for one minute out of every four. Winds were observed at the surface buoys (sites 1, 2, 3) and at the meteorological shore station (site W).

2.1. Winds

[6] Upon landfall, Hurricane Juan was traveling at 15 m/s with a central pressure of 97.3 kPa. The fast forward motion of the storm caused the wind field to be strongly asymmetric, with 20 m/s offshore winds on the west side of the track in Lunenburg and 44 m/s onshore winds on the eastern side near Halifax. The wind field at the time of landfall is shown in the inset of Figure 1, predicted from a parametric wind model developed from the theory of Holland [1980] for a

two-dimensional Rankine vortex. Wind observations in Lunenburg Bay at site 2, adjusted to the 10 m elevation (Figure 2a), show that southeast winds (directed into the bay) preceded the maximum wind conditions, and that the wind direction rapidly veered anticlockwise with the passage of the storm center, consistent with the vortex model predictions for the west side of the storm track.

2.2. Water Levels

[7] The water level observations at site 2 are shown in Figure 2b, including the tide and storm surge. Prediction of the astronomical tide was conducted according to Pawlowicz *et al.* [2002] using data from a pressure sensor at 10 m depth. A continuous 30 day record of average 30 minute pressure

Table 1. Instruments in Lunenburg Bay in 2003 With Water Depth, Sampling Frequency, and Sampling Interval^a

Site	Instrument	Waves/ Currents	h , m	f_s , Hz	Interval, min
<i>D</i>	DataWell directional waverider buoy	w	30	1.28	30
<i>A</i>	RDI Waves ADCP (1.2 MHz)	w + c	19	2.00	120
1	RDI Waves ADCP (1.2 MHz)	w + c	13	2.00	30
2	Sontek ADP (1.5 MHz)	c	10	1.00	30
	Seabird pressure sensor	w	10	0.62	30
3	Sontek ADP (1.5 MHz)	c	12	1.00	30
	Seabird pressure sensor	w	12	0.62	30
4	InterOcean S4	c	21	2.00	1-min avg.
5	InterOcean S4	c	8	2.00	1-min avg.
6	InterOcean S4	c	12	2.00	1-min avg.

^aWater depth, h ; sampling frequency, f_s .

was used, and 96.6% of the variance was accounted for by the tides, using 29 tidal constituents in the analysis. Residual water levels were determined from the difference between observations and predictions. The peak storm surge occurred only 1 hour after a spring high tidal water elevation of 0.87 m above mean sea level (MSL). The maximum storm surge was 0.65 m, consistent among observations at sites *A*, 2 and 3. The combined (tide + surge) water levels reached approximately 1.5 m above MSL uniformly within the bay.

2.3. Waves

[8] The significant wave height (H_s) observations for Hurricane Juan are shown in Figure 2c, and are not uniformly distributed within the bay. Waves outside the bay observed at site *D* approached the bay from due south, the peak wave period reached 14 s and H_s reached 9.2 m at maximum. Inside the bay, H_s values were smaller, attenuated by refraction and wave breaking. Waves with H_s greater than 4 m reached the mouth of the bay at observation sites *A* and 1.

2.4. Currents

[9] Depth-averaged mean current magnitudes at four observation sites are shown in Figure 2d. Strong outflow currents of 0.2–0.3 m/s were observed at sites *A*, 1 and 3 near the mouth of the bay, with near-surface currents of up to 0.4 m/s at *A* and 1. The currents lagged the peak in wave energy by 1–2 hours, and were two to three times stronger than typical tidal currents of ≤ 0.1 m/s.

[10] At site 2, depth-averaged currents were weak, < 0.05 m/s during the event. Near-bottom currents were observed at sites 4–6 (Figure 1). Site 4 was located in a deep bathymetric channel ($h = 21$ m), and bottom currents were a maximum of 0.12 m/s southward along the N-S trending channel axis. Site 5 was located near the north shore ($h = 12$ m) and bottom currents were weak, < 0.05 m/s during the event. Site 6 was located outside the tidal channel ($h = 8$ m) and bottom currents were strong (0.30 m/s ebb, 0.05 m/s flood) and aligned with the channel axis.

3. Coupled Numerical Model

[11] Delft3D is a hydrodynamic modeling package developed by WL|Delft Hydraulics in the Netherlands. *Elias et al.* [2000] describe validation of the model in 2D (depth-averaged mode), for an alongshore uniform coast

in the Netherlands. They obtained good agreement with measurements, and were able to simulate wave-driven longshore and rip currents associated with bar bathymetry. *Lesser et al.* [2004] described the development and validation of the 3D flow model, including simulation of sediment transport and morphology change.

[12] The Delft3D model has been used to simulate tidal, wind, and wave-driven flow conditions in Lunenburg Bay. The model bathymetry was derived from a high-resolution multibeam mapping survey completed in 2006, and grids were developed with 60 m resolution. Waves and currents are computed by separate but coupled models within Delft3D, as briefly outlined in the following sections.

3.1. Wave Model

[13] The SWAN model [*Booij et al.*, 1999] is a third-generation shallow-water spectral wave model that includes wave propagation, refraction due to currents and depth, generation by wind, dissipation (whitcapping, bottom friction, depth-induced breaking), and nonlinear wave-wave interactions. The model conserves wave action density $N(\sigma, \theta)$, equal to energy density $E(\sigma, \theta)$ divided by the relative wave frequency σ . The relative wave frequency σ is related to the fixed wave frequency ω by the wave number vector \mathbf{k} and mean current vector \mathbf{u} ,

$$\sigma = \omega - \mathbf{k} \cdot \mathbf{u}. \quad (1)$$

The evolution of the wavefield in SWAN is described by the action balance equation

$$\frac{\partial}{\partial t} N + \frac{\partial}{\partial x} (c_x + u)N + \frac{\partial}{\partial y} (c_y + v)N + \frac{\partial}{\partial \sigma} c_\sigma N + \frac{\partial}{\partial \theta} c_\theta N = \frac{S_{tot}}{\sigma}, \quad (2)$$

which describes the local rate of change of action density with time, t , and the propagation of action density in each dimension. Velocities c_x and c_y are spatial x and y components of the group velocity c_g , the speed at which wave action is transported. c_θ and c_σ are the rates of change of c_g , which describe the directional (θ) rate of turning and frequency shifting due to changes in currents (u , v) and water depth. Wave propagation on the left-hand side of equation (2) is balanced by local changes to the wave spectrum from energy density source terms S_{tot} on the right-hand side, which describe the sources, sinks and distribution of energy in the wave spectrum [*Booij et al.*, 1999]. Radiation stresses are determined from spatial gradients in the directional energy spectrum $E(\sigma, \theta)$. The strongest gradients in radiation stress occur owing to depth-induced breaking. The energy dissipation rate for wave breaking is expressed by the *Battjes and Janssen* [1978] model,

$$D_{tot} = -\frac{1}{4} \alpha_{BJ} Q_b \left(\frac{\bar{\sigma}}{2\pi} \right) H_{max}^2, \quad (3)$$

where $\alpha_{BJ} = 1$, Q_b is the fraction of breaking waves [*Booij et al.*, 1999], $\bar{\sigma}$ is the mean frequency and H_{max} is the maximum wave height that can exist in a given water depth determined from $H_{max} = \gamma h$, where the breaking parameter

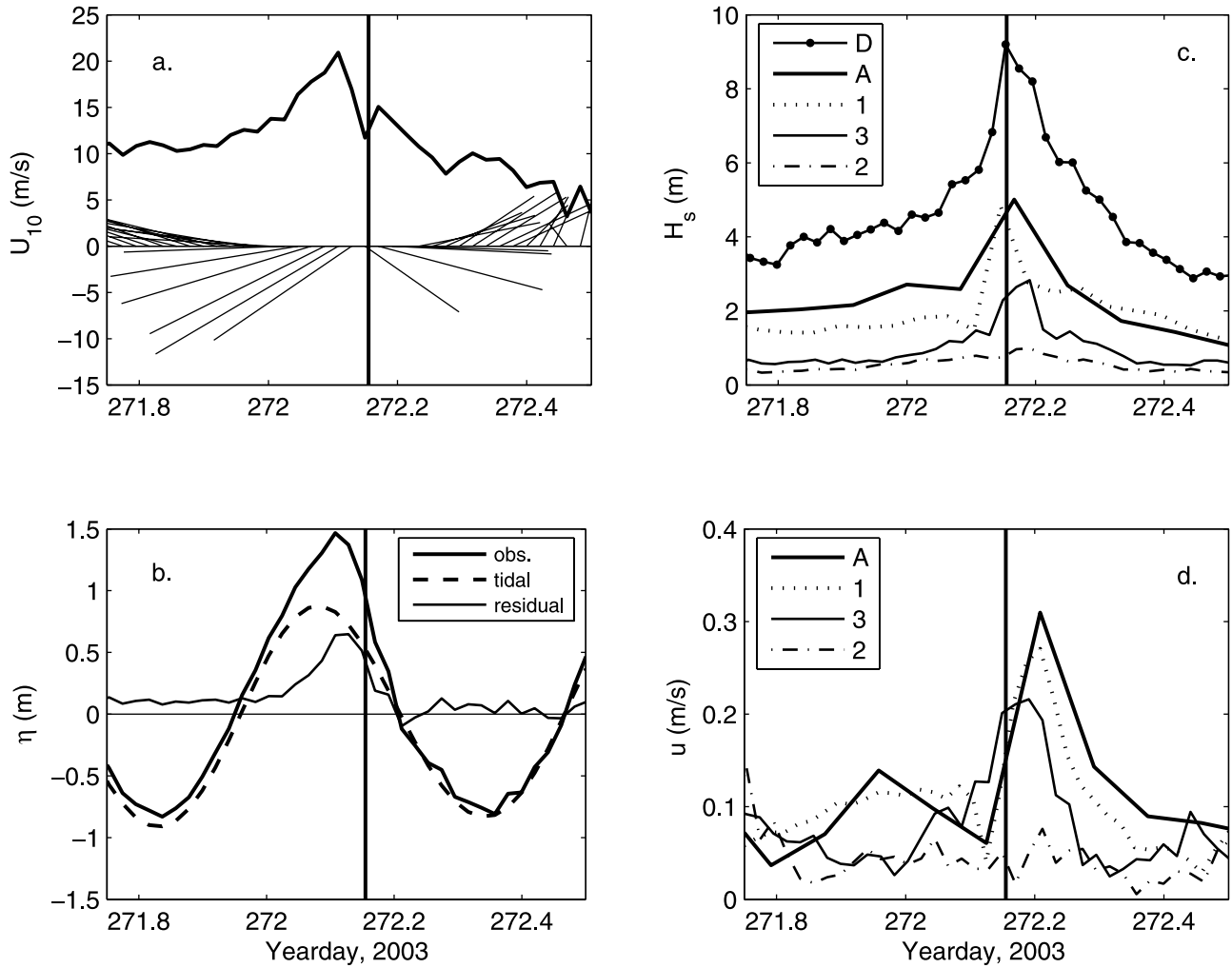


Figure 2. Observations in Lunenburg Bay during Hurricane Juan: (a) wind speed and wind vectors at site 2; (b) observed water level, tidal component, and residual water levels at site 2 (peak storm surge was 0.65 m); (c) significant wave height; and (d) depth-averaged current magnitude. Vertical reference line indicates the time of peak wave height at site D (YD 272.15, 29 September at 0330 UTC).

$\gamma = 0.73$. The contribution from depth-induced breaking to the total source term S_{tot} in equation (2) is

$$S_{br}(\sigma, \theta) = \frac{D_{tot}}{E_{tot}} E(\sigma, \theta). \quad (4)$$

[14] SWAN has been validated against observations in Lunenburg Bay by *Mulligan et al.* [2008] for a case of an extratropical storm with combined swell and wind-sea conditions, when offshore H_s reached a maximum of 3.8 m. The observed currents were less than 0.2 m/s, and currents were not included in the wave model computations. In the present application, wave-current interaction is included in the wave simulations. The wave model was implemented on a rectangular grid (Figure 1), covering an area of 13.7 km in the east-west (x) direction and 10.4 km in the north-south (y) direction with a resolution of 60 m. It was configured with frequencies in 49 logarithmic bins

from 0.03 to 3.00 Hz ($\Delta\sigma/\sigma = 0.1$), and direction bins in $\Delta\theta = 10^\circ$ increments. The time series of wave spectra observed at site D were applied uniformly along open wave boundaries. The wave model was run in stationary mode with a time step of 30 min using observed waves at the boundaries, observed winds and water levels over the domain and currents from the flow model. The assumption of stationarity is valid for the given domain size and time step for the long-period swell entering the model domain through the boundary [*Mulligan et al.*, 2008]. The swell is responsible for wave breaking and wave-generated currents in the bay.

3.2. Flow Model

[15] The finite difference flow model was applied to Lunenburg Bay to numerically solve the horizontal momentum equations [*Lesser et al.*, 2004] in 2D including forcing by waves, water levels and winds. Delft3D accounts for the effects of waves on mean flow by: (1) including radiation stress gradients [*Longuet-Higgins and Stewart*, 1964] in the flow momentum equations; (2) enhancing the bed shear

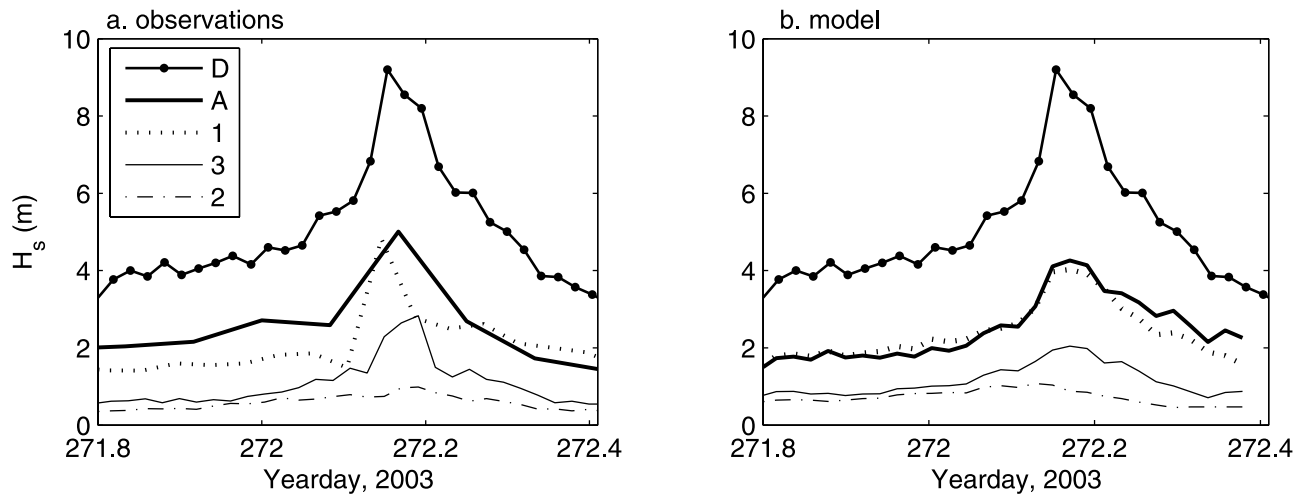


Figure 3. Time series of significant wave height at the five sites shown on Figure 1: (a) observations and (b) model predictions.

stress due to waves [Fredsoe, 1984]; (3) inducing turbulence and vertical mixing [Lesser *et al.*, 2004]; and (4) accounting for Stokes drift using a generalized Lagrangian mean approach [Groeneweg and Battjes, 2003].

[16] For Lunenburg Bay, the flow domain covered an area of 10.7 km in the east-west (x) direction and 8.2 km in the north-south (y) direction with a resolution of 60 m. The flow domain was constructed inside the larger wave model domain (Figure 1) to allow waves to adjust within the wave domain before reaching the flow domain. This avoided unrealistically strong wave-driven currents due to breaking near the boundary, since the wave model used observations from site *D* uniformly along the open boundaries (and h is variable along the boundaries). Water level elevation boundary conditions were applied as time series along the open boundaries of the flow domain.

[17] To examine both the combined and separate effects of each type of forcing, six model runs were conducted: (model A) combined wave, wind and water level (tide + surge) forcing; (model B) wave forcing only; (model C) tide, surge and wind forcing; (model D) tide and surge forcing; (model E) tidal forcing only; and (model F) local wind forcing only. Each model was run for a period of 15 hours when H_s was greater than or equal to 3 m outside the bay, from YD 271.8 to 272.4 (see Figure 2c), using default parameter settings for horizontal eddy viscosity, bottom roughness and wind drag. The flow model operated

with a time step of 30 s and paused for communication with the wave model at 30 minute intervals.

4. Model Results

4.1. Wave Predictions

[18] Time series of observed and predicted H_s at the instrument sites are shown in Figure 3, and are presented in Table 2 for YD 272.15. The model captured the general trend of decreasing wave energy from the most exposed sites (*A* and 1) to most protected site (*2*). The comparison is not as good at site 3, in the vicinity of the south headland. Refraction, either by depth or currents or both, was not adequately calculated by the model in this area, since the observed H_s is larger than predictions. This could be due to inaccurate bathymetry in the model (in areas shallower than 5 m, where the high-resolution bathymetry survey was not conducted) or to current-induced refraction. It is suspected that the observed long-period waves were refracted into the area by either shallow water depths or by strong horizontal shear of the opposing current. The wavefield is shown in Figure 4 at the time of peak wave energy, YD 272.15, when $H_s = 9.2$ m outside the bay at site *D*. The spatial distribution of wave height (Figure 4a) shows that the headland on the south side and the north shore of the bay were exposed to large waves. This is also evident from estimates of the wave energy dissipation rate (Figure 4b). Dissipation, overwhelmingly due to depth-induced breaking, was strongest at the

Table 2. Observations and Predictions for Waves and Currents^a

Site	$H_{sObs.}$	$H_{sPrediction}$	$\bar{u}_{Observation}$	\bar{u}_A	\bar{u}_B	\bar{u}_C	\bar{u}_D	\bar{u}_E	\bar{u}_F
D	9.2	-	-	-	-	-	-	-	-
A	5.0	4.2	0.23	0.29	0.24	0.12	0.08	0.07	0.06
1	4.5	4.1	0.20	0.18	0.25	0.08	0.06	0.05	0.06
2	0.9	1.0	0.05	0.06	0.07	0.04	0.05	0.03	0.03
3	2.3	1.9	0.17	0.17	0.14	0.13	0.08	0.06	0.06

^aSignificant wave height (m) is given at the time of peak wave conditions (YD 272.15); depth-mean outflow current magnitude (m/s) is averaged over the period YD 272.1–272.3 for each model run. A: wave, tide, surge, wind; B: wave; C: tide, surge, wind; D: tide,surge; E: tide; F: wind.

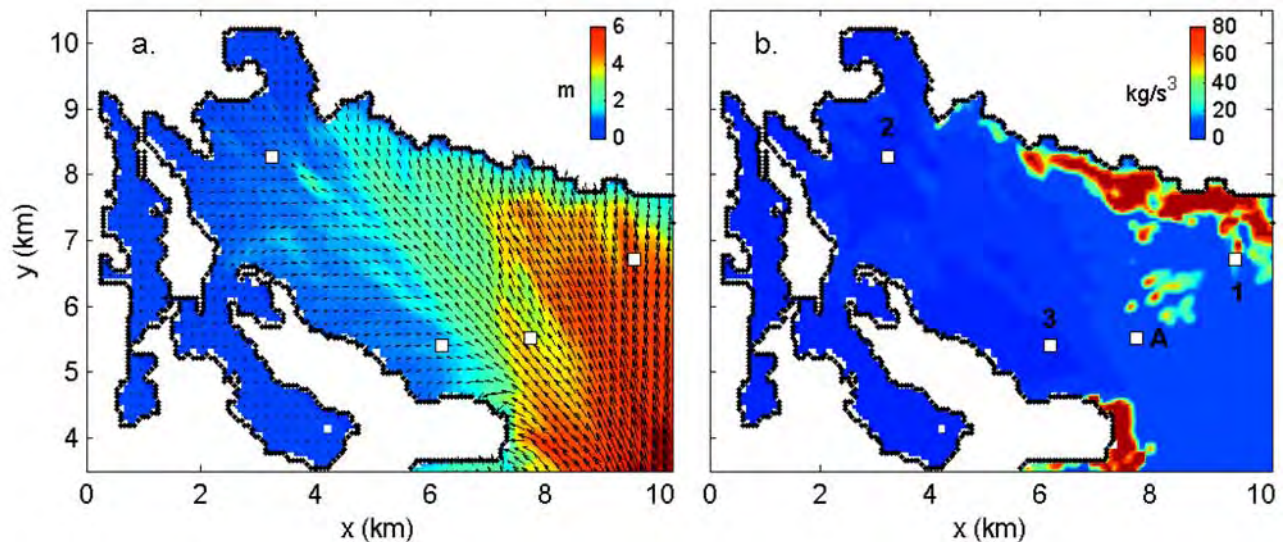


Figure 4. Wave model results in selected portion of model grid at the time of peak wave energy, YD 272.15 (29 September at 0330 UTC with offshore $H_s = 9.2$ m): (a) significant wave height (gray scale) and direction vectors and (b) wave energy dissipation rate. Vectors are subsampled at $1/3$ model resolution, and squares represent instrument locations.

south headland and along the north shore. In addition, wave breaking occurred over the shoal near the mouth of the bay.

4.2. Current Predictions

[19] Currents for each model run are presented in Figures 5 and 6. In Figure 5, time series from each model run are compared to observed currents at the three sites that span the mouth of the bay. A very similar pattern existed in the observed currents at sites 1 and A: inflow preceded the wave energy peak and was associated with the tide and surge forcing; strong outflow was mainly wave-driven. During the time of highest waves, wave-driven flow dominated and the observations and predictions are in agreement. Prior to this when the flow was significantly weaker, wave flows and tidal flows are of similar magnitude, but model predictions were not always in agreement with observations. The discrepancies could be due to 3D effects such as opposing wave and tidal flows, or to local bathymetric steering of currents not resolved by the model.

[20] Figure 6 shows the current field for selected model runs at the time of peak current magnitude, YD 272.2, illustrating horizontal variability in the currents for each forcing type. Tide + surge forcing (Figure 6d) induced a strong jet from the tidal channel in the western end of the bay, and outflow in the eastern end was uniform across the bay. The predicted wind currents and tidal currents shown here compare well with recent model simulations of Wang *et al.* [2007].

[21] The combined model incorporated all three forcing types (wave, tide + surge, and wind, Figure 6a), and captured the major features of the bay circulation, including the magnitude, direction and timing of currents. Table 2 presents a summary of the current speeds averaged over the period YD 272.1–272.3, when flow was directed out of the bay (+x direction). The results demonstrate that the combined model best matches the observations, and waves were the dominant process forcing the low-frequency motions.

[22] The model results are consistent with the observed near-bottom currents at sites 5 and 6. At site 5 currents were weak at 12 m depth, and therefore not strongly influenced by the longshore current which occurred in <10 m depth along the north shore. At site 6 the currents were strong, and forced by tide and surge. At site 4, the depth-averaged current magnitude was well predicted by the model, but the direction was not. The model predicted outflow directed to the east, however observations showed that currents went southward owing to local bathymetric steering in the deep channel.

[23] Wave energy dissipation, mainly due to wave breaking, generated radiation stress gradients and induced strong mean flows in the bay. Inflowing wave-driven longshore currents were predicted along the north shore and south headland, shown in Figure 6b. The longshore current was predicted to have been considerably wider on the north shore, as it was exposed to larger waves and has shallower bathymetry. Strong outflow occurred in the center of the bay, and was weaker on the north side owing to the influence of the shoal to the east. While the observed currents at site A and site 1 are notably similar in magnitude and direction (Figures 5a and 5b), the model results indicated that the horizontal currents were different at these sites, located in different bathymetric channels on opposite sides of the shoal. To summarize, the wave-driven inflow was directly driven by the radiation stress gradients mainly along the north coast, and the wave-driven outflow in the deeper channels was a result of mass balance of the wave-driven inflow.

[24] Delft3D was used in 2D mode for the runs presented here, but has 3D capability. The 2D implementation allowed the depth-averaged flow to be directly determined. Currents measured by acoustic profiling instruments during the time period of Hurricane Juan had a simple vertical structure that had near-uniform velocity and direction with depth. As a

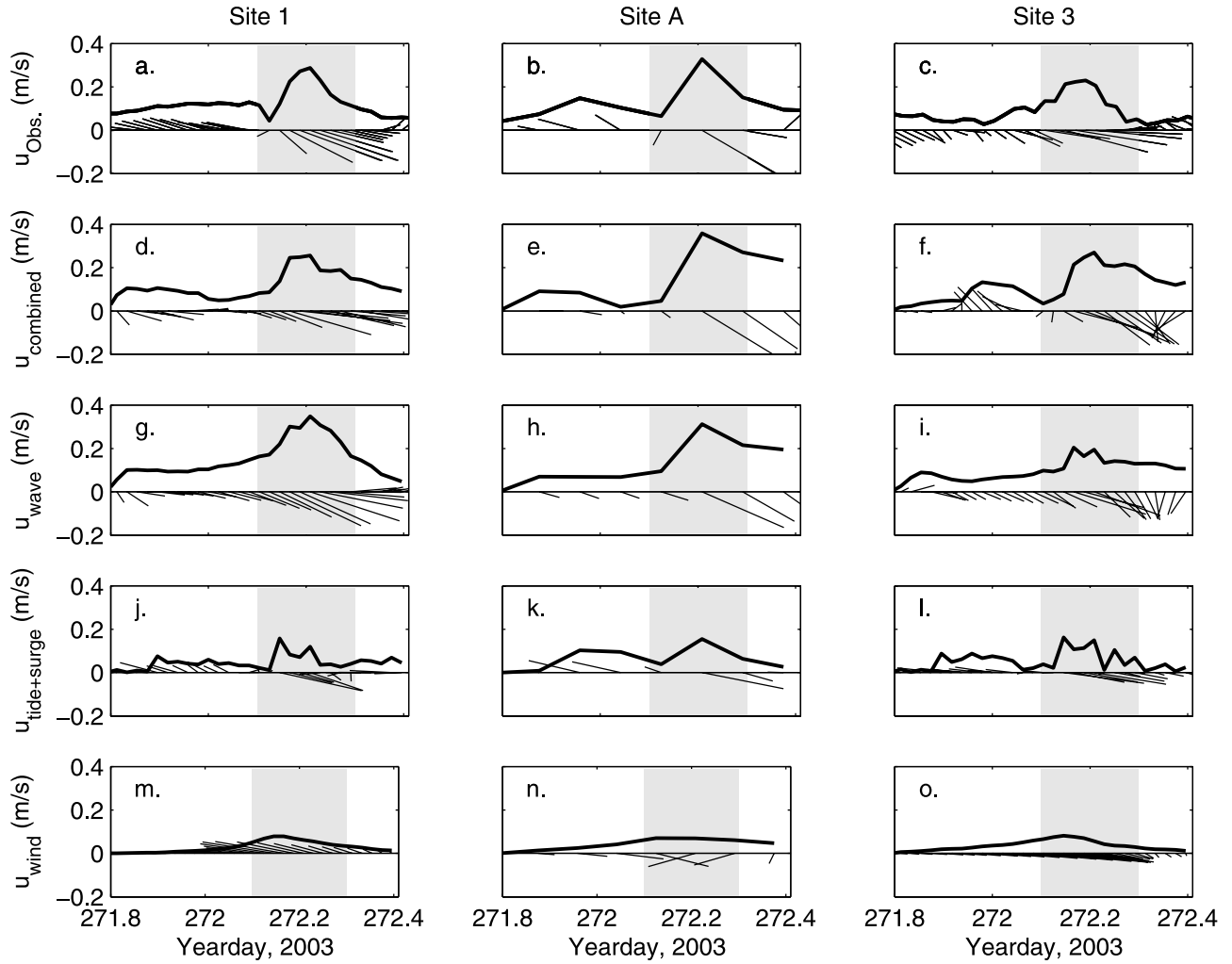


Figure 5. Depth-averaged currents at three instrument locations. (a–c) Observations. (d–f) Run A: combined wave/tide/surge/wind forced model. (g–i) Run B: wave forced model. (j–l) Run D: tide and surge forced model. (m–o) Run F: wind forced model. Data and model results shown every 0.5 h at Sites 1 and 3, and model subsampled at a 2-h interval to match observations at Site A. Thick lines show current magnitude and stick vectors show both magnitude and direction. Gray area is time period from YD 272.1–272.3 when offshore H_s exceeded 5 m.

test to examine the vertical structure of the predicted currents, run A was repeated in 3D mode with 10 vertical layers using a sigma coordinate system. The depth-averaged mean flow results from the 3D test run were equivalent to the 2D results.

4.3. Flushing Rates

[25] The flushing rate is the rate at which water in the bay is replaced by water from outside, as opposed to movement of existing water within the bay. Flushing depends not only on the magnitude and direction of currents, but also the time and length scales over which the currents act. Using the modeled depth-averaged currents, flushing rates can be estimated and used to determine the contribution of surface wave forcing to the total exchange of water. To examine the balance of inflows and outflows, a transect across the model domain in the y direction, oriented south-to-north (see Figure 6) was considered. The volumetric flow rate of water

through the transect in the $+x$ direction (outflow) was estimated by

$$Q^+(t) = \sum_{i=1}^n h_i(y) u_i^+(y, t) dy, \quad (5)$$

where $i = 1$ at the south end of the transect, $i = n$ at the north end, h is the water depth along the transect, u^+ is the outflow velocity perpendicular to the transect and dy is the model grid cell size. Similarly, Q^- describes the volumetric flow rate in the $-x$ direction (inflow). Along this 3.6 km transect with a mean depth of 12.2 m, each forcing type had a significantly different horizontal velocity structure, shown for YD 272.2 in Figure 6. The inflow and outflow rates are given in Table 3 at selected times: (1) 4 hours before peak outflow, on flood tide; (2) at peak outflow; and (3) 4 hours after peak outflow. Flows estimated from model run D (tide + surge)

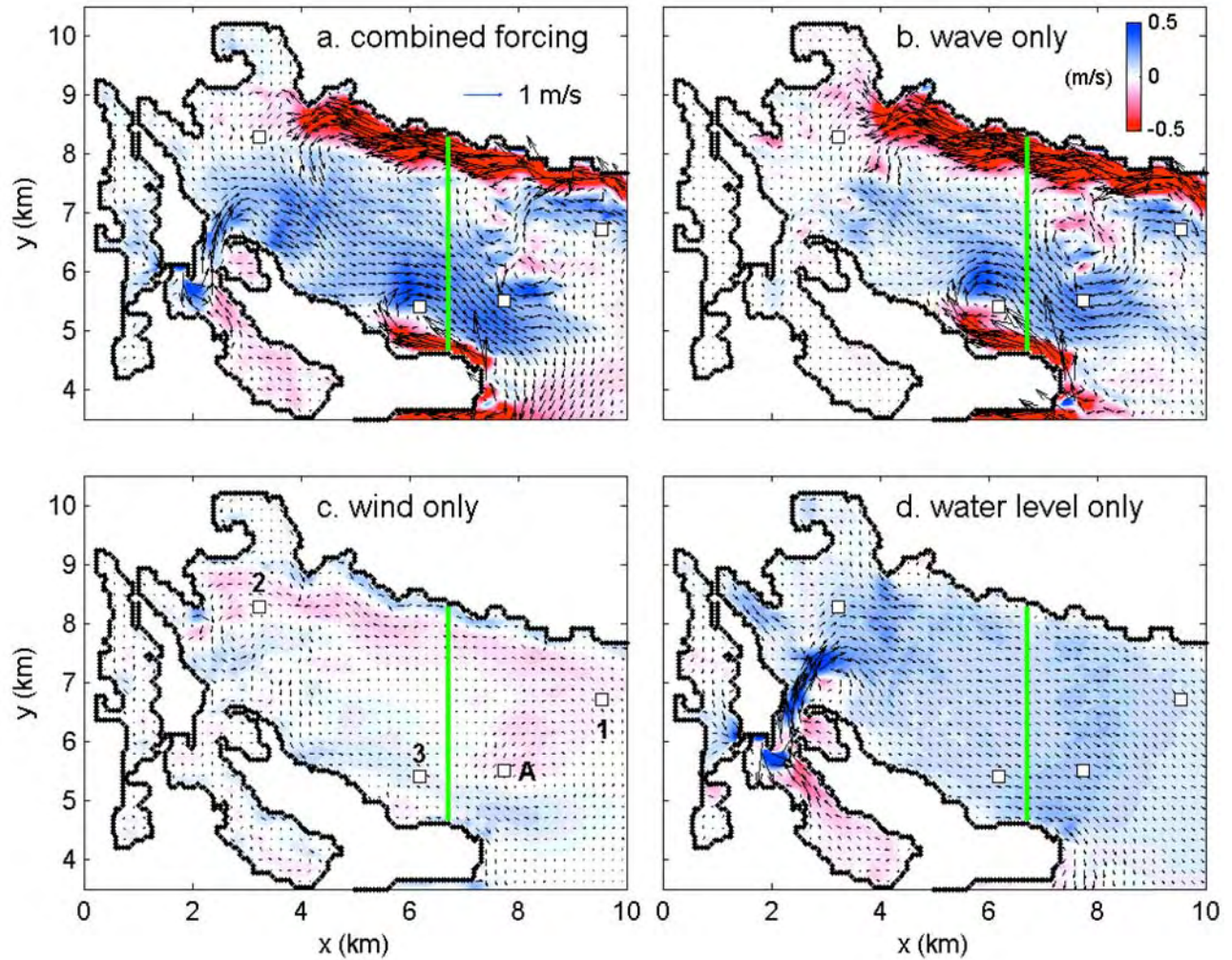


Figure 6. Current vectors and false-color u component in selected portion of model grid at the time of peak current magnitude, YD 272.2 (29 September at 0500 UTC), predicted by the flow model. (a) Run A: combined wave/tide/surge/wind forcing. (b) Run B: wave forcing only. (c) Run F: local wind forcing only. (d) Run D: water level (tide and surge) forcing only. Red represents flow in the $-x$ direction and blue represents flow in the $+x$ direction. Vectors are subsampled at $1/3$ model resolution, and squares represent instrument locations and the green line is the transect location.

Table 3. Volumetric Flow Rates Through the Transect for Model Runs^a

YD	Q , m ³ /s	A	B	C	D	E	F
272.04	Q^-	-3669	-1577	-2381	-2457	-1370	-677
	Q^+	1027	1486	0	0	25	631
272.21	Q^-	-3718	-5293	-2	-8	0	-543
	Q^+	7280	5134	5007	5244	2609	699
272.38	Q^-	-3161	-2699	-870	-867	-1812	-283
	Q^+	3347	2561	221	0	0	422
272.21	k_{50} (m)	200	180	1660	3500	3600	400
	k_0 (m)	1050	600	3600+	3600+	3600+	1250
271.88–272.38	$\Delta V/V_b$	0.57	0.53	0.24	0.23	0.17	0.11

^aModel runs A–F are listed in Table 2. At selected times, correlation length scales and total volume exchanged over the 0.5-day period.

indicate that water flowed in or out of the bay in one direction at a given time, on a timescale of 12 hours for a complete cycle. These flows balanced, i.e., $Q^+ = Q^-$, over the 0.5-day period from $t_1 = \text{YD } 271.88$ to $t_2 = \text{YD } 272.38$. Model run F showed that wind introduced horizontal variability to the circulation across the bay. The wind-driven flow rates, which were smaller than tidal flow rates, balanced over a much shorter timescale of only ~ 1 hour. Wave-driven flows (run B) during Hurricane Juan had the largest flow rates in the bay, with strong horizontal gradients. The wave-driven flows balanced on a timescale of 1–2 hours, providing the strongest circulation mechanism.

[26] For each model run, spatial autocorrelation functions were computed, shown in Figure 7. The correlation length scales k_{50} and k_0 were estimated by finding the lag distance k at which the autocorrelation function $R(k)$ for flow Q intersects the 50% and 0% levels. The correlation length scales at

YD 272.2 are given in Table 3. These values demonstrate that wave-driven flows vary strongly over short horizontal distances ($k_{50} < 200$ m), wind-driven flows vary over intermediate scales ($k_{50} \sim 400$ m), and tide- and storm-surge-driven flows vary over length scales on the order of the bay width ($k_{50} > 3600$ m). Anticorrelation ($k_0 < 0$) occurs for wave- and wind-driven flows, indicating that flows in opposing directions occur along the transect at a given time. Anticorrelation does not occur for tide- and surge-driven flows, since flow is unidirectional along the transect.

[27] To determine the volume of water exchanged between the bay and ocean, the volumetric flow rate passing through the transect over the 0.5-day period was integrated. Since $Q^+ = Q^-$ over the storm event, the volume of water exchanged can be defined as $\Delta V = \Delta V^+ = \Delta V^-$, in terms of either the inflow or outflow volume. The volume exchanged is estimated by

$$\Delta V = \int_{t_1}^{t_2} Q^+(t) dt, \tag{6}$$

where dt is the model time step. The fraction of bay volume exchanged was determined by $\Delta V/V_b$ where V_b is the total bay volume west of the transect, approximately 2.3×10^8 m³. The volume fractions are given in Table 3. Wave-driven flow was the major contributor to the exchange of water. For tidal forcing only (tidal water levels shown in Figure 2b), representing a typical spring tide, the volume exchanged was 17%. The volume exchanged during the hurricane estimated from the combined model was 57%, more than three times the maximum possible flushing capacity of a typical tidal cycle. The short cross-bay correlation length scale of the wave-driven circulation, together with the fact that inflow and outflow balance across the bay over timescales of 1–2 hours, indicate that most of the wave-driven volume

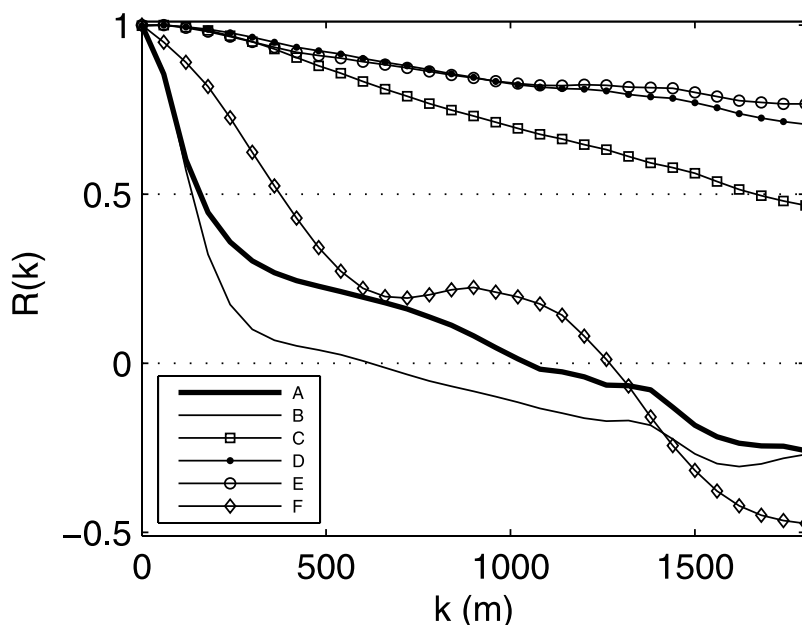


Figure 7. Lagged autocorrelation functions for Q along the transect shown in Figure 6 for model runs listed in Table 2 at YD 272.2 (29 September at 0500 UTC).

exchange represents flushing as opposed to movement of water within the bay. Conversely the tides, for which the volume exchange contributes to flushing mainly as a result of mixing [Dyer, 1973], are nearly uniform across the bay and act over a longer timescale of 12 hours. Nonlinearity in the system is indicated by the volume fractions in Table 3, as the model results for each forcing type do not sum to the result given by run A with combined forcing.

5. Conclusions

[28] The passage of a hurricane accompanied by high waves (>9 m offshore) induced strong currents in a coastal bay. Wave breaking, which occurred in shallow areas along the shore and over a shoal at the bay entrance, induced a circulation that varied over small $O(0.1-1 \text{ km})$ horizontal scales. Observations at three locations provided evidence of outflow currents, and the wave-driven flow model was used to estimate the circulation pattern within the bay. The wave-driven inflow was directly driven by the radiation stress gradients, mainly along the north shore. The wave-driven outflow, in the deeper channels, was a result of the mass balance of the wave-driven inflow and lagged the time of peak inflow and wave height. Wave-driven flows were stronger than currents driven by tides, storm surge and wind, and significantly increased volumetric flow rates in the bay, acting over a timescale that was shorter than a tidal cycle. Numerical prediction of the inflow and outflow rates indicate that over 50% of the bay volume was exchanged during the storm. The short cross-bay correlation length scale of the wave-driven circulation, together with the fact that inflow and outflow balance across the bay, indicate that most of the wave-driven volume exchange represents flushing as opposed to movement of water within the bay. Thus the results presented here demonstrate that the wave-forced circulation can provide a more efficient flushing mechanism in the bay than tides. These results indicate that wave-driven currents should be included in coastal circulation models for prediction of oceanographic conditions during wave events.

[29] **Acknowledgments.** We thank Doug Schillinger at Dalhousie University for instrument setup, calibration, and data management, and Peter Smith and Will Perrie at the Bedford Institute of Oceanography for cooperation and sharing of directional waverider and ADCP data. Use of the model is gratefully acknowledged, as part of the Delft3D Community Model Development Project sponsored by WL| Delft Hydraulics and the U.S. Office of Naval Research. This study was funded by the Canadian Foundation for Climate and Atmospheric Sciences and the Natural Sciences and Engineering Research Council of Canada.

References

- Battjes, J., and J. Janssen (1978), Energy loss and set-up due to breaking of random waves, paper presented at 16th International Conference on Coastal Eng., Am. Soc. of Civ. Eng., Hamburg, Germany.
- Booij, N., R. Ris, and L. Holthuijsen (1999), A third-generation wave model for coastal regions: 1. Model description and validation, *J. Geophys. Res.*, *104*(4), 7649–7666.
- Bowen, A. (1969), Rip currents: 2. Laboratory and field observations, *J. Geophys. Res.*, *74*(23), 5479–5490.
- Dyer, K. (1973), *Estuaries: A Physical Introduction*, John Wiley, Hoboken, N. J.
- Elias, E., D. Walstra, J. Roelvink, M. Stive, and M. Klein (2000), Hydrodynamic validation of Delft3D with field measurements at Egmond, paper presented at 27th International Conference on Coastal Engineering, Am. Soc. of Civ. Eng., Sydney.
- Fedderson, F., and R. Guza (2003), Observations of nearshore circulation: alongshore uniformity, *J. Geophys. Res.*, *108*(C1), 3006, doi:10.1029/2001JC001293.
- Fredsoe, J. (1984), Turbulent boundary layer in wave-current interaction, *J. Hydraul. Eng.*, *110*, 1103–1120.
- Gourlay, M., and G. Colleter (2005), Wave-generated flow on coral reefs—An analysis for two-dimensional horizontal reef-tops with steep faces, *Coastal Eng.*, *52*, 353–387.
- Groeneweg, J., and J. Battjes (2003), Three-dimensional wave effects on a steady current, *J. Fluid Mech.*, *478*, 325–343.
- Holland, G. (1980), An analytic model of the wind and pressure profiles in hurricanes, *Mon. Weather Rev.*, *108*, 1212–1218.
- Kraines, S., T. Yanagi, M. Isobe, and H. Komiyama (1998), Wind-wave driven circulation on the coral reef at Bora Bay, Miyako Island, *Coral Reefs*, *17*, 133–143.
- Lesser, G., J. Roelvink, J. van Kester, and G. Stelling (2004), Development and validation of a three-dimensional morphological model, *Coastal Eng.*, *51*, 883–915.
- Longuet-Higgins, M., and R. Stewart (1964), Radiation stresses in water waves; a physical discussion, with applications, *Deep Sea Res.*, *11*, 529–562.
- Mulligan, R. P., A. J. Bowen, A. E. Hay, A. J. van der Westhuysen, and J. A. Battjes (2008), Whitecapping and wave field evolution in a coastal bay, *J. Geophys. Res.*, *113*, C03008, doi:10.1029/2007JC004382.
- Pawlowicz, R., B. Beardsley, and S. Lentz (2002), Classical tidal harmonic analysis including error estimates in MATLAB using T-TIDE, *Comput. Geosci.*, *28*, 929–937.
- Sheng, J., and L. Wang (2003), A high-resolution coastal circulation model for Lunenburg Bay, Nova Scotia, paper presented at 8th International Conference on Estuarine and Coastal Modelling, Am. Soc. of Civ. Eng., Monterey, Calif.
- Sheng, J., and L. Wang (2004), Numerical study of tidal circulation and nonlinear dynamics in Lunenburg Bay, Nova Scotia, *J. Geophys. Res.*, *109*, C10018, doi:10.1029/2004JC002404.
- Sturley, D., and A. Bowen (1996), A model for contaminant transport in Lunenburg Bay, Nova Scotia, *Sci. Total Environ.*, *179*, 161–172.
- Symonds, G., K. Black, and I. Young (1995), Wave-driven flow over shallow reefs, *J. Geophys. Res.*, *100*(C2), 2639–2648.
- Wang, L., J. Sheng, A. Hay, and D. Schillinger (2007), Storm-induced circulation in Lunenburg Bay of Nova Scotia: Observations and numerical simulations, *J. Phys. Oceanogr.*, *37*, 873–895.

A. J. Bowen, A. E. Hay, and R. P. Mulligan, Department of Oceanography, Dalhousie University, 1355 Oxford Street, Halifax, NS, Canada B3H 4J1. (mulligan@phys.ocean.dal.ca)